Synthesis, crystal structure and solid-state dynamics of the La(hfa)₃·Me(OCH₂CH₂)₄OMe (Hhfa = 1,1,1,5,5,5-hexafluoropentane-2,4-dione) precursor for MOCVD applications

Graziella Malandrino,[a] **Ignazio L. Fragalà,**[*,a] **Silvio Aime,**[*,b] **Walter Dastrù,**[b] **Roberto Gobetto**[b] **and Cristiano Benelli**[c]

[a] *Dipartimento di Scienze Chimiche, Università di Catania, V.le Andrea Doria 6, 95125 Catania, Italy*

[b] *Dipartimento di Chimica Inorganica, Chimica Fisica e Chimica dei Materiali, Università di Torino, Via Pietro Giuria 7, 10125 Torino, Italy*

[c] *Dipartimento di Chimica, Università di Firenze, Via Maragliano 77, 50144 Firenze, Italy*

The reaction of La₂O₃ with 1,1,1,5,5,5-hexafluoropentane-2,4-dione (Hhfa) and tetraglyme [Me(OCH₂CH₂)₄OMe] in hexane yielded the air stable, ten-co-ordinate La(hfa)₃·Me(OCH₂CH₂)₄OMe adduct. This new adduct represents a promising volatile lanthanum precursor for low-pressure MOCVD applications. It displays a high volatility, which can be related to a fast molecular reorientation in the solid state as established by combined DSC, ¹H and ¹³C NMR investigations.

The growing demand for novel precursors for metal-organic chemical vapour deposition (MOCVD) applications has recently stimulated the design of novel co-ordination architectures and the search for new synthetic strategies.[1–7] The MOCVD precursors act as gas-phase carriers for the metallic atoms from the condensed phase to the target device. High thermal stability upon evaporation, high vapour pressure and constant mass transport properties are prerequisite characteristics for these complexes. Such properties have been found in several alkaline[1–5] and rare-earth[6,8–10] β-diketonate complexes whose co-ordination spheres are saturated with ancillary polyether ligands. In particular, the use of fluorinated β-diketones has been shown to produce highly volatile and thermally stable lanthanide precursors.[8,10] In fact, the presence of fluorine enhances the volatility of the adducts while co-ordinated polyethers prevent water co-ordination and oligomerization.

In this context, we report the synthesis, structure and physicochemical properties of the novel adduct formed between La(hfa)₃ (Hhfa = 1,1,1,5,5,5-hexafluoropentane-2,4-dione) and tetraglyme (tetraglyme = 2,5,8,11,14-pentaoxapentadecane) which exhibits good mass transport properties. The possible relationship between its volatility and the remarkable molecular mobility below the melting point is addressed.

Results and Discussion

The single step reaction of lanthanum oxide with Hhfa and tetraglyme in hexane yields the air stable ten-co-ordinate adduct, La(hfa)₃·Me(OCH₂CH₂)₄OMe **1**, see Scheme 1. It quantitatively evaporates in the range 95–100 °C (10⁻⁴ mmHg = 133.322 × 10⁻⁴ Pa).

The ORTEP[11] drawing of La(hfa)₃·Me(OCH₂CH₂)₄OMe is shown in Fig. 1 and selected bond distances and angles are reported in Table 1. Single-crystal X-ray diffraction data for **1** point to a mononuclear complex in which a ten-co-ordinate lanthanum atom is encapsulated by the six oxygen atoms of the (hfa)₃ cluster and four (of the potential five) O-donor atoms of the tetraglyme. The unco-ordinated oxygen atom is located far from the metal ion (5.460 Å). The co-ordinated polyhedron surrounding the La ion is described by a distorted bicapped antiprism with O(6) and O(9) in the capping positions.[12] The average La–O (hfa) distance (2.533 Å) is identical to that observed in the La(hfa)₃·O(CH₂CH₂OMe)₂ analogue

Table 1 Selected bond lengths (Å) and angles (°) for La(hfa)₃·Me(OCH₂CH₂)₄OMe

La(1)–O(4)	2.501(4)	La(1)–O(2)	2.515(3)
La(1)–O(5)	2.528(4)	La(1)–O(1)	2.536(4)
La(1)–O(3)	2.544(4)	La(1)–O(6)	2.579(4)
La(1)–O(10)	2.682(4)	La(1)–O(8)	2.710(4)
La(1)–O(11)	2.724(4)	La(1)–O(9)	2.753(4)
O(4)–La(1)–O(2)	136.01(13)	O(4)–La(1)–O(5)	78.67(14)
O(2)–La(1)–O(5)	143.65(13)	O(4)–La(1)–O(1)	135.36(13)
O(2)–La(1)–O(1)	66.91(12)	O(5)–La(1)–O(1)	80.02(13)
O(4)–La(1)–O(3)	67.63(13)	O(2)–La(1)–O(3)	127.73(13)
O(5)–La(1)–O(3)	68.3(2)	O(1)–La(1)–O(3)	136.26(14)
O(4)–La(1)–O(6)	67.35(13)	O(2)–La(1)–O(6)	111.30(14)
O(5)–La(1)–O(6)	66.8(2)	O(1)–La(1)–O(6)	68.27(14)
O(3)–La(1)–O(6)	120.80(14)	O(4)–La(1)–O(10)	68.21(14)
O(2)–La(1)–O(10)	75.05(13)	O(5)–La(1)–O(10)	140.10(14)
O(1)–La(1)–O(10)	139.61(13)	O(3)–La(1)–O(10)	78.6(2)
O(6)–La(1)–O(10)	116.3(2)	O(4)–La(1)–O(8)	136.96(13)
O(2)–La(1)–O(8)	81.97(13)	O(5)–La(1)–O(8)	72.44(14)
O(1)–La(1)–O(8)	69.76(13)	O(3)–La(1)–O(8)	72.31(14)
O(6)–La(1)–O(8)	125.1(2)	O(10)–La(1)–O(8)	118.6(2)
O(4)–La(1)–O(11)	76.20(13)	O(2)–La(1)–O(11)	65.43(13)
O(5)–La(1)–O(11)	131.1(2)	O(1)–La(1)–O(11)	89.43(14)
O(3)–La(1)–O(11)	134.1(2)	O(6)–La(1)–O(11)	64.9(2)
O(10)–La(1)–O(11)	61.9(2)	O(8)–La(1)–O(11)	146.46(13)
O(4)–La(1)–O(9)	113.34(14)	O(2)–La(1)–O(9)	63.52(13)
O(5)–La(1)–O(9)	119.52(14)	O(1)–La(1)–O(9)	111.30(14)
O(3)–La(1)–O(9)	64.22(13)	O(6)–La(1)–O(9)	173.6(2)
O(10)–La(1)–O(9)	59.5(2)	O(8)–La(1)–O(9)	59.16(14)

Scheme 1

½ La₂O₃ + 3 Hhfa + tetraglyme ⟶
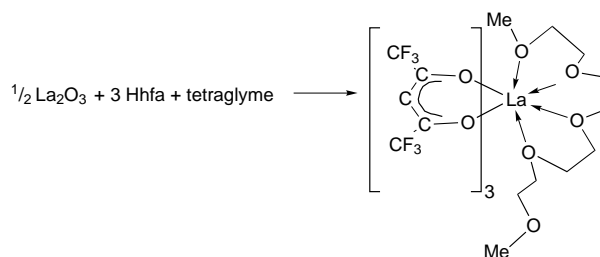
(2.533 Å).[8] The average La–O (ether) distance (2.717 Å) appears significantly larger than in the O(CH₂CH₂OMe)₂ homologue (2.547 Å).[8] It compares well with the values
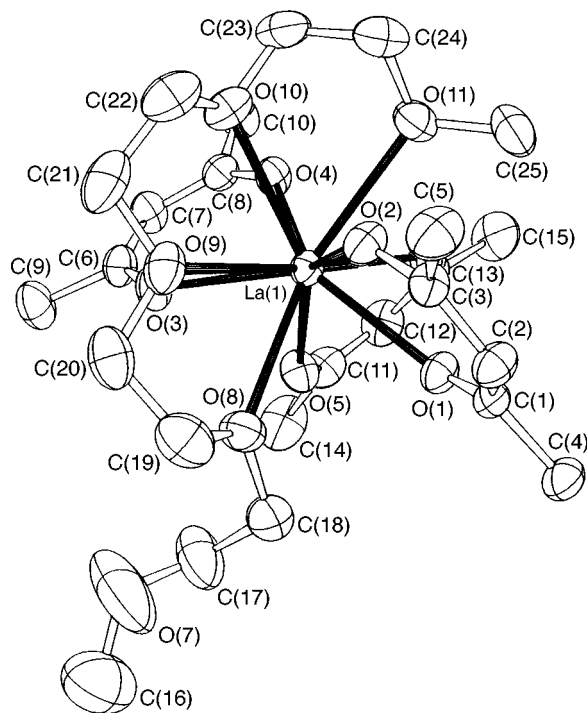
Fig. 1 An ORTEP drawing of the crystal structure of the La(hfa)$_3$·Me-(OCH$_2$CH$_2$)$_4$OMe adduct; CF$_3$ groups have been omitted for clarity
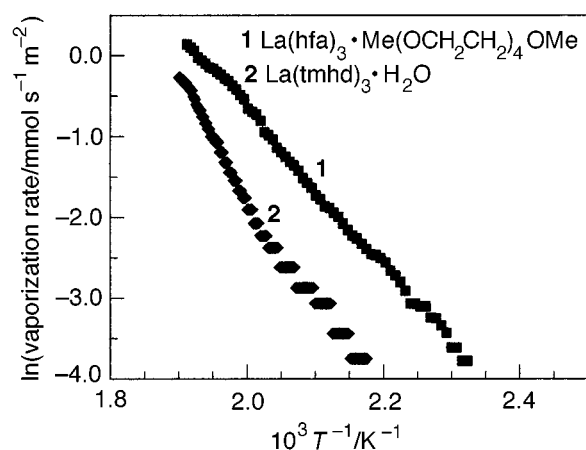
Fig. 2 Atmospheric-pressure vaporisation rate TG data of La(hfa)$_3$·Me-(OCH$_2$CH$_2$)$_4$OMe compared to La(tmhd)$_3$·H$_2$O as a function of temperature

reported for both the ten-co-ordinated lanthanum(III) adducts with ethereal oxygens [13] as well as for the nine-co-ordinated La(tmhd)$_3$·Me(OCH$_2$CH$_2$)$_4$OMe species (2.706 to 2.781 Å, Htmhd = 2,2,6,6-tetramethylheptane-3,5-dione).[6] It should, however, be noted that the similar La–O (ether) bond values of the La(hfa)$_3$·Me(OCH$_2$CH$_2$)$_4$OMe and La(tmhd)$_3$·Me(OCH$_2$-CH$_2$)$_4$OMe adducts, do not imply a similar thermal behaviour. In fact, La(hfa)$_3$·Me(OCH$_2$CH$_2$)$_4$OMe sublimes quantitatively *in vacuo*, while the adduct La(tmhd)$_3$·Me(OCH$_2$CH$_2$)$_4$OMe decomposes upon sublimation to yield the tmhd complex bereft of the tetraglyme ligand. This difference in behaviour is similar to that found for the barium homologues and can be explained in an analogous fashion.[3a]

Rate data of thermal gravimetric vaporisation of the present adduct at atmospheric pressure are reported in Fig. 2 and compared to the classical La(tmhd)$_3$·H$_2$O. The vaporisation rate of the tetraglyme adduct shows a linear behaviour, thus indicating a good thermal stability of the adduct in this temperature range even under atmospheric pressure. Note that in the highest temperature range (200–250 °C), the La(hfa)$_3$·Me(OCH$_2$-
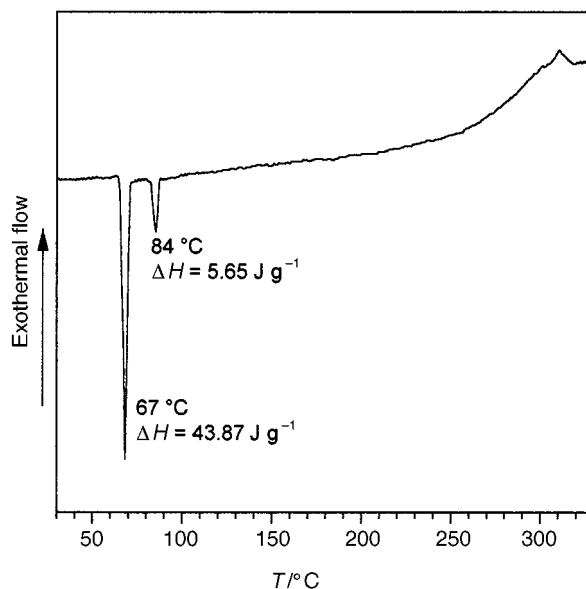
Fig. 3 The DSC curve of the La(hfa)$_3$·Me(OCH$_2$CH$_2$)$_4$OMe adduct
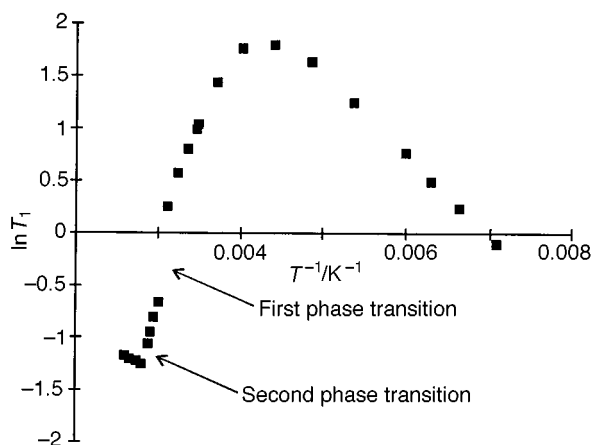
Fig. 4 Variation of proton spin–lattice relaxation times T_1 with inverse temperature (K^{-1}) for La(hfa)$_3$·Me(OCH$_2$CH$_2$)$_4$OMe

CH$_2$)$_4$OMe adduct vaporises *ca.* 3 times more rapidly than La(tmhd)$_3$·H$_2$O. At lower temperature, the volatility of the tetraglyme adduct compared to La(tmhd)$_3$·H$_2$O is even more pronounced and in fact, the tetraglyme adduct begins to sublime, under atmospheric pressure, 60 °C below La(tmhd)$_3$·H$_2$O.

Differential scanning calorimetric (DSC) analysis and optical microscopy indicate that the La(hfa)$_3$·Me(OCH$_2$CH$_2$)$_4$OMe adduct undergoes a reversible phase transition at 67 °C and that it completely melts at 84 °C (Fig. 3).

The DSC behaviour is in close accordance with proton longitudinal relaxation time T_1 (NMR) measured under wideline mode over an extended temperature range. Data in Fig. 4 show clear evidence of two T_1 drops corresponding to the phase-transition temperatures observed in the DSC thermograph. Moreover, the T_1 profile provides an indication that at low temperature, the T_1 values are governed mainly by the rotation of the methyl groups (E_a from the slope ≈4.2 kJ mol^{-1}).[14] On going from room to higher temperatures, the enhanced relaxation rates indicate that there are molecular motions which relax the proton sink more efficiently than the methyl rotation. The T_1 discontinuity observed at 67 °C indicates a phase transformation characterised by a higher molecular mobility. At 83 °C the system undergoes a second transition corresponding to the melting point and, subsequently, any further temperature increase causes a slow T_1 increase as expected for a liquid phase. These observations prompted us to undertake high-resolution ^{13}C NMR investigations to gain more insight into the dynamic
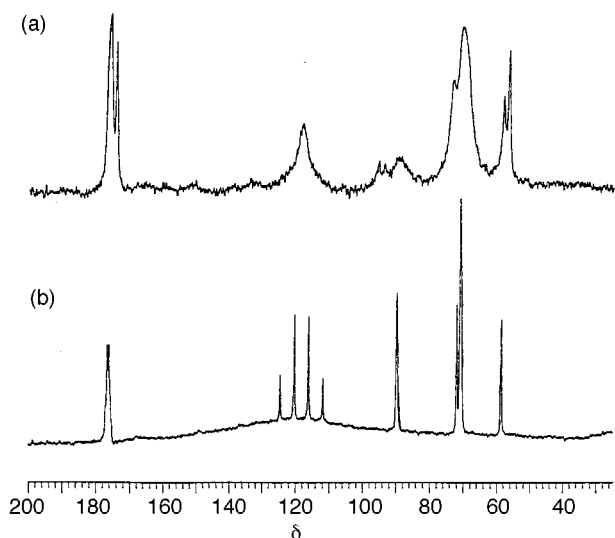
Fig. 5 Carbon-13 NMR spectra of La(hfa)$_3$·Me(OCH$_2$CH$_2$)$_4$OMe: (a) CP-MAS at room temperature; (b) MAS-{^{1}H} at 70 °C
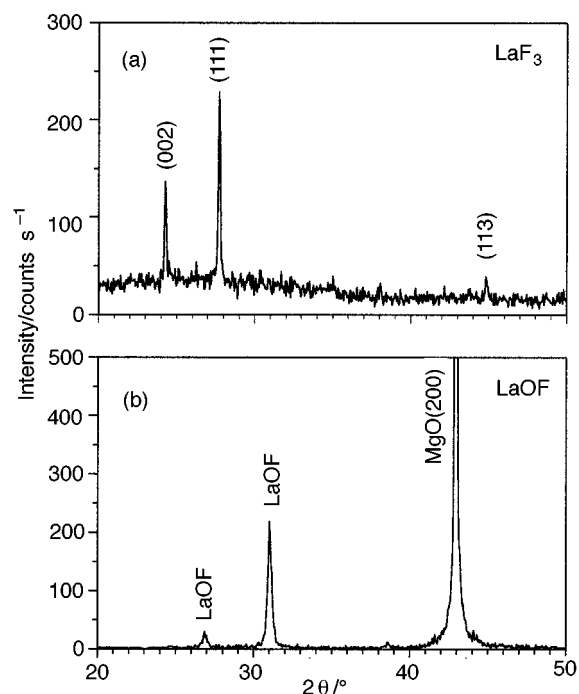

Fig. 6 X-Ray diffraction patterns of MOCVD-grown LaF$_3$ films on glass substrates (550 °C) (a) and LaOF films on MgO (100) substrates (750 °C) (b) using the La(hfa)$_3$·Me(OCH$_2$CH$_2$)$_4$OMe adduct

features accompanying the first phase transition. The room-temperature ^{13}C-CPMAS NMR spectrum [Fig. 5(a)] displays several broad resonances whose associated chemical shifts are similar to those found in solution. The two asymmetric high field resonances (δ 55.8 and 58.0 respectively) due to the unco-ordinated methoxy moieties, point to unequally populated structures differing in the lay-out of the tetraglyme moiety. Above 67 °C the ^{13}C-MAS-{^{1}H} NMR spectrum [Fig. 5(b)] shows a dramatic sharpening of all the resonances with the complete disappearance of any spinning sideband pattern[15] thus suggesting the occurrence of a phase characterised by an extensive molecular mobility. Furthermore, the sharpening of the ^{13}C resonances parallels an overall simplification of the spectral pattern, which becomes almost superimposable on the solution spectrum. In particular, the two asymmetric high-field methoxy resonances previously mentioned coalesce into a single sharp peak. This observation suggests that the overall dynamic process may not involve an extensive intramolecular rearrangement of the co-ordination cage or, at least, it does not exchange co-ordinated and unco-ordinated methoxy groups of the tetraglyme moiety.

In the context of MOCVD applications it is interesting to relate the solid molecular dynamics to the volatility of this type of complex. It appears that the remarkably fast molecular reorientation observed in the 67–85 °C temperature interval is evidence for loose packing constraints in the solid, below the melting point. Actually the ΔH value accompanying the phase transition at 67 °C ($\Delta H = 43.87$ J g^{-1}) is much larger than that measured at the melting temperature ($\Delta H = 5.65$ J g^{-1}).

Preliminary low-pressure MOCVD experiments, carried out on glass and MgO substrates from the La(hfa)$_3$·Me(OCH$_2$-CH$_2$)$_4$OMe adduct, yielded lanthanum-containing films. The X-ray diffraction pattern of a film deposited at 550 °C on a glass substrate under O$_2$ flow, shows the formation of a lanthanum trifluoride (LaF$_3$) phase [Fig. 6(a)]. At higher temperature (750 °C) a humid oxygen flow partially hydrolyses the LaF$_3$ to lanthanum oxofluoride (LaOF) [Fig. 6(b)]. The peaks at 26.85 and 31.00° can be associated with LaOF of various crystalline forms (cubic, tetragonal or rhombohedral), while the peak at 42.95° is associated with the MgO (200) reflection. Further experiments are clearly needed to discriminate between the types of crystalline structure of LaOF films grown in the present MOCVD experiments. Note that analogous polyether complexes [namely La(hfa)$_3$·O(CH$_2$CH$_2$OMe)$_2$ and La(hfa)$_3$·Me(OCH$_2$CH$_2$)$_3$OMe] have been used as MOCVD precursors for the deposition of high quality LaAlO$_3$.[16]

In summary, present data focus on the potential capabilities of combined calorimetric and NMR experiments to probe *a priori* novel molecular systems for MOCVD applications. Further studies on the relation between volatility/mass-transport properties and the solid-state molecular dynamics are in progress in our laboratory.

Experimental

Materials

Commercial La$_2$O$_3$, Hhfa and tetraglyme (Aldrich) were used without any further purification.

Physical measurements and instrumentation

Elemental microanalyses were performed in the Analytical Laboratories of the University of Catania. Proton NMR spectra were recorded on a Bruker 200 Fourier-transform spectrometer. Infrared data were collected on a 684 Perkin-Elmer Spectrometer from either Nujol or hexachlorobutadiene mulls of the sample between KBr plates. Thermal measurements were made using a Mettler 3000 system equipped with a TG 50 thermobalance, a TC 10 processor and DSC 30 calorimeter. Masses of the samples were between 15 and 20 mg (TG) and 4 and 10 mg (DSC). Analyses were carried out under prepurified nitrogen using 10 °C min^{-1} (TG) and 5 °C min^{-1} (DSC) heating rates. Fast atom bombardment mass spectra were obtained using a Kratos MS 50 spectrometer.

Wideline H-spin–lattice relaxation times (T_1) were measured using the inverse recovery pulse sequence on a JEOL GSE-270 spectrometer operating at 270 MHz. Solid-state ^{13}C NMR spectra were recorded at 67.8 MHz using cross-polarization magic angle spinning (CPMAS). In a typical experiment the CP contact time was 3 ms, the recycle times 15 s, and the spinning speed range between 4.0 and 5.0 kHz. In the experiment at 70 °C no CP was possible and the spectrum was recorded under the MAS mode only.

Synthesis

La(hfa)$_3$·Me(OCH$_2$CH$_2$)$_4$OMe 1. The compound La$_2$O$_3$ (6.3 mmol) was first suspended in hexane (150 ml) and tetraglyme

Empirical formula	C$_{25}$H$_{25}$F$_{18}$LaO$_{11}$
M	982.36
T/K	293(2)
λ/Å	0.71 069
Crystal system	Monoclinic
Space group	$P2_1/n$
a/Å	9.343(2)
b/Å	20.236(2)
c/Å	19.889(2)
β/°	90.39(8)
U/Å^3	3760.2(10)
Z	4
D_c/Mg m^{-3}	1.735
μ/mm^{-1}	1.275
$F(000)$	1928
Crystal size/mm	0.25 × 0.42 × 0.36
Crystal colour	Colorless
θ range/°	2.60–25.93
Index ranges	$-11 \leqslant h \leqslant 11$,
	$0 \leqslant k \leqslant 24$,
	$0 \leqslant 1 \leqslant 24$
Reflections collected	7481
Independent reflections	7269 [R(int) = 0.0289]
Refinement method	Full-matrix least-squares on F^2
Data, restraints, parameters	7269, 0, 498
Goodness-of-fit on F^2	1.260
Final R indices [$I > 2\sigma(I)$]	$R1 = 0.0553$, $wR2 = 0.1573$
R indices (all data)	$R1 = 0.0755$, $wR2 = 0.1729$
Largest difference peak, hole/e Å^{-3}	1.41, −1.194
Weighting scheme	w = 1/[$\sigma^2(F_o^2) + (0.1P)^2$] where $P = (F_o^2 + 2F_o^2)/3$
Shift/esd mean value	0.018

(11.7 mmol) was added to the suspension. On addition of Hhfa (35.3 mmol) the La$_2$O$_3$ immediately dissolved. The excess of lanthanum oxide was removed by filtration. After a slight reduction of the solution volume, colourless crystals separated and were collected by filtration and dried under vacuum. Yield 88%, m.p. (crude product) 81–84 °C. ^{1}H NMR (200 MHz, CDCl$_3$): δ 3.34 (s, 6 H, OCH$_2$), 3.68 (m, 8 H, OCH$_2$), 3.88 (s, 8 H, OCH$_2$), 6.01 (s, 3 H, CH). ^{13}C NMR (50 MHz, CDCl$_3$): 59.4 (s, OCH$_3$), 70.6 (s, OCH$_2$), 70.8 (s, OCH$_2$), 72.0 (s, OCH$_2$), 90.8 (s, CH), 117.7 (q, ^1J = 286, CF$_3$), 175.9 (q, ^2J = 34 Hz, CO). MS (dry FAB): m/z 775 (100%, [$M -$ hfa]$^+$), 587 (11, [$M - 2$hfa + F]$^+$), 553 (<5, [$M -$ hfa $-$ L]$^+$), 399 (6, [$M - 3$hfa + 2F]$^+$), 365 (<5, [$M - 2$hfa $-$ L + F]$^+$) (Found: C, 30.59; H, 2.64. Calc. for C$_{25}$H$_{25}$F$_{18}$O$_{11}$La: C, 30.55; H, 2.56%).

Crystal structure determination

Complex **1** was recrystallized from hexane. The colorless crystal, of dimensions 0.25 × 0.3 × 0.4 mm, was mounted at the end of a quartz fiber. X-Ray data were collected on an Enraf-Nonius CAD 4 four-circle diffractometer, using Mo-Kα radiation. Unit-cell parameters were derived from a least-squares refinement of a set of 25 reflections in the 8 < θ < 16° range and are reported in Table 2 with other experimental parameters. Corrections were applied for Lorentz and polarization effects but not for absorption. The reflections were processed by the direct method program SIR 92[17] to determine the position of the La atom and of the co-ordinated oxygen atoms. The other atomic parameters were determined by conventional Fourier-difference syntheses and the whole set was refined using the SHELXL 93[18] package. The final results are listed in Table 2. Anisotropic displacement parameters were introduced for all non-hydrogen atoms. The hydrogen atoms were included as idealised atoms riding on the respective carbon atoms with C−H bond lengths appropriate to the carbon atom hybridisation. The isotropic displacement parameter of each hydrogen

atom was fixed at 1.25 times the equivalent parameter of the carbon to which it was bonded.

Final results for the adduct show, without any constraint or special model, some distortion from the idealised geometry. Some evidence of disorder was observed around the oxygen atom not bonded to lanthanum [O(7)]. An attempt to improve the quality of the final structure solution was made assuming that this atom and the two bonded carbon atoms were divided over two equivalent positions each with a half integer occupancy factor. No substantial improvement in R factor was observed and, therefore, these atoms were refined normally. In the final stage of refinement, a pair of peaks with intensity approximately around 1.15 e Å^{-3} were observed close to the lanthanum atom. The refinement converged to a final agreement factor $R = 0.0553$ [$I > 2\sigma(I)$] and $R = 0.0755$ for all data.

CCDC reference number 186/899.

MOCVD Experiments

Low-pressure MOCVD depositions of lanthanum-containing films were performed under Ar (carrier gas, 100 standard cm^3 min^{-1}) and dry or humid O$_2$ (reaction gas, 300 standard cm^3 min^{-1}) flow, using a horizontal hot-wall reactor from the La(hfa)$_3$·Me(OCH$_2$CH$_2$)$_4$OMe source. Magnesium(II) oxide and glass substrates were used for the deposition. The source temperature was controlled in the range 115–120 °C.

References

1 K. Timmer, K. I. M. A. Spee, A. Mackor, H. A. Meinema, A. L. Spek and P. Van der Sluis, *Inorg. Chim. Acta*, 1991, **190**, 109.
2 R. S. Drake, S. A. S. Miller and D. J. Williams, *Inorg. Chem.*, 1993, **32**, 3227.
3 (*a*) G. Malandrino, I. L. Fragalà, D. A. Neumayer, C. L. Stern, B. J. Hinds and T. J. Marks, *J. Mater. Chem.*, 1994, **4**, 1061; (*b*) S. H. Shamlian, M. L. Hitchman, S. L. Cook and B. C. Richards, *J. Mater. Chem.*, 1994, **4**, 81.
4 G. Malandrino, F. Castelli and I. L. Fragalà, *Inorg. Chim. Acta*, 1994, **224**, 203.
5 D. A. Neumayer, D. B. Studebaker, B. J. Hinds, C. L. Stern and T. J. Marks, *Chem. Mater.*, 1994, **6**, 878.
6 S. R. Drake, A. Lyons, D. J. Otway, A. M. Z. Slawin and D. J. Williams, *J. Chem. Soc., Dalton Trans.*, 1993, 2379.
7 T. J. Marks, *Pure Appl. Chem.*, 1995, **67**, 313.
8 G. Malandrino, R. Licata, F. Castelli, I. L. Fragalà and C. Benelli, *Inorg. Chem.*, 1995, **34**, 6233.
9 I. Baxter, S. R. Drake, M. B. Hursthouse, K. M. A. Malik, J. McAleese, D. J. Otway and J. C. Plakatouras, *Inorg. Chem.*, 1995, **34**, 1384.
10 G. Malandrino, O. Incontro, F. Castelli, I. L. Fragalà and C. Benelli, *Chem. Mater.*, 1996, **8**, 1292.
11 C. K. Johnson, ORTEP, Report ORNL-5138, Oak Ridge National Laboratory, Oak Ridge, TN, 1976.
12 S. P. Sinha, *Struct. Bonding* (Berlin), 1976, **25**, 69.
13 R. D. Rogers, A. N. Rollins, R. D. Etzenhouser, E. J. Voss and C. B. Bauer, *Inorg. Chem.*, 1993, **32**, 3451.
14 E. R. Andrew, R. Gaspar and W. Wennart, *Chem. Phys. Lett.*, 1976, **38**, 141.
15 C. F. Fyfe, *Solid State NMR for Chemists*, C. F. C. Press, Ontario, Canada, 1983.
16 G. Malandrino, I. L. Fragalà and P. Scardi, *Chem. Mater.*, submitted.
17 A. Altomare, G. Cascarano, C. Giacovazzo and A. Guagliardi, *J. Appl. Crystallogr.*, 1994, **27**, 1045.
18 G. M. Sheldrick, SHELXL 93, Program for Crystal Structure Determination, University of Göttingen, 1993.